Chemical Geology 640 (2023) 121748

Contents lists available at ScienceDirect

Chemical Geology

journal homepage: www.elsevier.com/locate/chemgeo

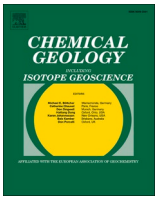

Pb diffusion in magnetite: Dating magnetite crystallization and the timing of remanent magnetization in banded iron formation

E. Bruce Watson [a,*], Daniele J. Cherniak [b], Claire I.O. Nichols [c], Benjamin P. Weiss [d]

[a] Rensselaer Center for Astrobiology Research and Education (RARE) and Department of Earth & Environmental Sciences, RPI, Troy, New York 12180, USA
[b] Department of Physics, University at Albany, State University of New York, 12222, USA
[c] Department of Earth Sciences, University of Oxford, South Parks Road, OX1 3AN, UK
[d] Department of Earth, Atmospheric and Planetary Sciences, MIT, Cambridge, MA 02139, USA

ARTICLE INFO

Editor: Marco Fiorentini

Keywords:
Magnetite
Pb diffusion
Banded iron formation (BIF)
Remanent magnetization
Closure temperature
U-Pb geochronology

ABSTRACT

The ferrimagnetic mineral magnetite (Fe_3O_4) is abundant in banded iron formation (BIFs), and has the potential to provide U—Pb or Pb—Pb age information on these rocks because it incorporates small amounts of U during growth. Combined with age measurements, paleomagnetic studies of BIF magnetites may also yield insight into the history of Earth's magnetic field and its relationship to early evolution of Earth's interior and atmosphere.

Reliable magnetite ages utilizing Pb isotopes require knowledge of Pb diffusion in the magnetite structure. For this reason, we undertook an experimental investigation of Pb diffusion in magnetite by diffusing Pb^{2+} ions into pre-polished slabs of natural magnetite oriented parallel to {001} or {111}. A mixture of $PbSO_4$ and Fe_2O_3 was used as a surface powder source to supply Pb^{2+} diffusant at the sample surface and at the same time buffer the oxygen fugacity of the system at magnetite-hematite (MH)—a typical f_{O2} for banded iron formations (BIFs) due to the common presence of both iron oxides (and where Pb^{2+} is stable relative to other Pb valence states). Diffusion experiments spanned temperatures of 500–675 °C and durations of 75 to 2035 h. Following each experiment, in-diffused Pb was depth-profiled using Rutherford backscattering spectroscopy (RBS) and Pb diffusivities were calculated from the profiles using an infinite half-space diffusion model. The following diffusion law for Pb^{2+} in magnetite is based upon 12 independent diffusivity measurements:

D_{Pb} ($m^2 \cdot s^{-1}$) = (9×10^{-17} $m^2 \cdot s^{-1}$) exp.(−98,000 $J \cdot mol^{-1}$)/RT)

where the uncertainties in the pre-exponential constant and activation energy are ±6% and ± 15%, respectively.

Pb diffusion in magnetite over the temperature range of our study is orders of magnitude slower than projected for other divalent cations based on down-temperature extrapolation of previously measured diffusion laws (e.g., for Mn^{2+}, Fe^{2+}, Co^{2+}, and Ni^{2+}). This finding is encouraging in terms of the potential suitability of magnetite for U—Pb age determinations of BIFs and other magnetite-bearing rocks. Indeed, classical Dodson closure temperatures well above 500 °C are not unrealistic in cases where magnetite crystals having large diffusion domains (e.g., >100 μm in radius) are cooled relatively rapidly (e.g., at 100 °C/MYr). This is of particular significance for paleomagnetic studies, since the Curie temperature of magnetite is 580 °C and therefore the age of magnetization in magnetite-bearing rocks may be directly dated. However, slow cooling of magnetites having small diffusion domains can lead to Pb loss at temperatures of 200 °C or lower. Pb mobilization is evaluated for various time-temperature scenarios that involve both heating and cooling as well as "closed-loop" time-temperature paths. We conclude that U—Pb or Pb—Pb age determinations of BIF magnetites are potentially reliable, but isotopic results should be assessed in concert with knowledge of the thermal history of the host rock and the effective grain size of the magnetites.

* Corresponding author.
E-mail address: watsoe@rpi.edu (E.B. Watson).

https://doi.org/10.1016/j.chemgeo.2023.121748
Received 15 June 2023; Received in revised form 18 September 2023; Accepted 22 September 2023
Available online 26 September 2023

1. Introduction

Knowledge of Pb diffusion in magnetite crystals from ancient banded iron formation (BIF) is important for several reasons. For example, because BIFs precipitate from seawater under oxidizing conditions, U—Pb (or Pb—Pb) dating of BIF-hosted magnetite can provide time constraints on the oxygenation of the oceans and atmosphere. In addition, because magnetite acquires natural remanent magnetism (NRM) when crystallized in a magnetic field below the Curie temperature (580 °C), BIF magnetites may document the existence of an intrinsic terrestrial magnetite field in the deep geologic past. In a broad sense, BIF magnetites have the potential to provide valuable input to the record of Earth's ancient dynamo by shedding light on the timing of thermal and thermochemical remnant magnetization (TRM and TCRM) and the influence of any subsequent thermal overprints. Knowledge of Pb diffusion in magnetite is needed to fully realize this potential in order to understand the relationship between U—Pb age of the magnetite and age of the NRM carried by the magnetite.

Direct age determinations of BIFs can be challenging because these materials generally lack phases well suited to traditional radioisotopic dating techniques. This challenge has led some researchers to evaluate the potential of iron oxides themselves (mainly magnetite [Fe_3O_4] but also hematite [Fe_2O_3]) as candidates for age determinations using the U—Pb or Pb—Pb methods, given that U can be incorporated in these minerals in modest amounts during crystallization (See Supplementary document S1 for a literature summary of Pb—Pb dating of magnetite. See also S2 for data on U and Pb concentrations in natural magnetites). Sufficient concentrations of radiogenic Pb (Pb*) and limited common Pb should enable determination of reliable radiometric ages (Erel et al., 1997; Frei et al., 1999; Frei and Polat, 2007; Courtney-Davies et al., 2022), provided Pb is effectively retained in the magnetite structure following initial crystallization. [Importantly, diffusion is not the only process capable of compromising Pb in BIF magnetites, which can be subject to recrystallization and/or hydrothermal alteration. However, diffusion is perhaps uniquely amenable to laboratory characterization, and can play a role in Pb behavior even if superimposed on other processes].

At the intrinsic oxygen fugacity of metamorphosed BIF (assumed to contain both hematite and magnetite—a solid-state f_{O2} buffer), the stable oxidation state of lead is Pb^{2+}. No diffusion data for Pb^{2+} in magnetite have been available up to this point, but other divalent cations (e.g., Ni^{2+}, Co^{2+}, Fe^{2+}, Mn^{2+}) are known to diffuse quite fast (leading to closure temperatures of 200–250 °C even for mm-sized grains), possibly suggesting poor retention of Pb in magnetite in geologic settings. This prediction is highly uncertain, however, because all existing cation diffusion data were obtained at temperatures in excess of 900 °C, which means that large down-temperature extrapolations are needed to address diffusion at temperatures that might have been experienced by a metamorphosed BIF. In addition, the ionic radius of Pb^{2+} is 40–70% larger than those of other divalent cations (e.g., Ni^{2+}, Co^{2+}, Mn^{2+}, Fe^{2+}) whose diffusion laws have been characterized (Van Orman and Crispin, 2010)—possibly foretelling more sluggish behavior of Pb^{2+} and better thermal retention in magnetite.

The present contribution describes the results of experiments aimed at characterizing Pb^{2+} diffusion in magnetite over a temperature range of 500° to 675 °C, which is directly relevant to the question of Pb retention in natural BIF over geologic time.

2. Samples and preparation

The magnetite crystals used in this study were from the town of Moriah in eastern Essex County, New York State, obtained from the RPI mineral collection. These crystals are shiny, black octahedra ranging up to ~1 cm in size and containing only minor impurities (see Table 1). They host occasional mineral inclusions, but these were readily avoided during analysis. Slabs of Moriah magnetite 5–8 mm^2 in area and ~ 1 mm thick were cut with a low-speed diamond saw to obtain slab surface orientations parallel to cubic {001} or octahedral {111} forms. The slabs were polished on one side to produce a surface suitable for in-diffusion of Pb, beginning with 600-grit SiC, progressing to 1 μm alumina powder, and finishing with colloidal silica. This stepwise procedure yielded a polished surface free of dislocations and other lattice damage that might have been introduced during sample cutting and initial coarse polishing (Watson et al., 2016).

Table 1
Moriah magnetite composition determined by electron microprobe (RPI Cameca SX100 operating at 15 kV; 20 nA; 1 μm beam spot). Fe_2O_3/FeO estimated from stoichiometry. Data are averages of two crystals.

oxide	wt%	σ; $n = 32$
Fe_2O_3	68.59	*
FeO	30.85	*
SiO_2	0.050	0.016
MnO	0.020	0.011
TiO_2	0.105	0.027
Al_2O_3	0.509	0.083
Cr_2O_3	0.01	0.010
MgO	0.10	0.020
V_2O_3	0.01	0.010
NiO	0.01	0.010

* Standard deviation for Fe as FeO = 0.56.

3. Methods

3.1. Experimental

The general strategy of the diffusion experiments was to pack the polished magnetite slabs in a Pb-bearing powder that would serve as a source of Pb^{2+} ions at the magnetite surface during high-temperature diffusion anneals. Mechanistically, Pb^{2+} was expected to diffuse into the magnetite in limited exchange for out-diffusing Fe^{2+}. The chosen Pb source was a mixture of $PbSO_4$ and Fe_2O_3 in a mass ratio of 1:1 or 1:2. These two compounds were pre-reacted at 900 °C for several hours before use in diffusion experiments; in some cases the Pb diffusion source in a particular diffusion experiment consisted of source powder recycled from an earlier run.

The specific choice of $PbSO_4$-Fe_2O_3 as our powder source was based partly on earlier success in our group using $PbSO_4$ as the source in a study of Pb diffusion in zircon (Cherniak and Watson, 2001). In the present case, our use of Fe_2O_3 as the diluent of $PbSO_4$ was strategic in the sense that the coexistence of this compound with the Fe_3O_4 diffusion sample constitutes a solid-state oxygen fugacity buffer (magnetite-hematite, or MH). This was advantageous because most BIFs contain both magnetite and hematite (Klein, 2001; Konhauser et al., 2017), and PbO is the stable oxidation state of Pb at the oxygen fugacity of the MH buffer (see Fig. 1). Buffering f_{O2} at MH insured that Pb was generally divalent in our experiments—as would be the case in BIFs—and that uptake of Pb in magnetite would logically take place in exchange for Fe^{2+}.

Diffusion experiments were set up by packing a polished magnetite slab in the Pb source powder inside a 5 × 7 mm SiO_2 glass tube that had been pre-sealed at one end. The tube was then evacuated and sealed off above the sample with an H_2-O_2 torch, and the length containing the sample was separated from the rest of the tube (by fusion) to create an evacuated ampoule 3–4 cm in length with sample and source inside (see Fig. 2). A diffusion anneal was conducted by hanging the ampoule in a vertical tube furnace, heating it to a predetermined temperature, holding for a prescribed duration, and quenching the ampoule in air by removal from the furnace. The experiments covered 500° to 675 °C, with durations ranging from 75 to 2035 h (see Table 2). Experiments below 500 °C were not practical because of the long duration required to produce measureable Pb uptake in the magnetite. Experiments above 675 °C resulted in reaction between the magnetite surface and the Pb

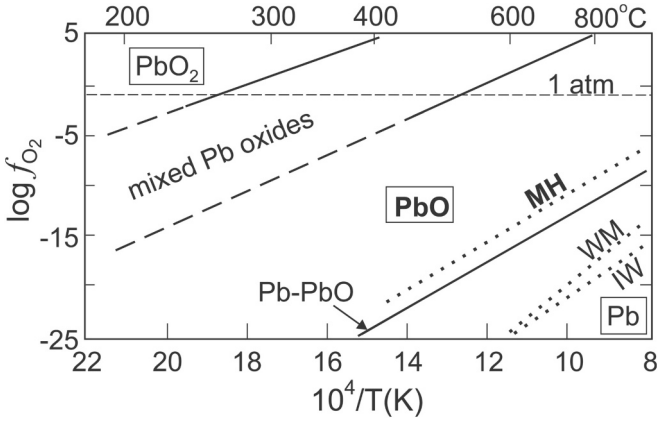

Fig. 1. Phases in the Pb—O system as a function of temperature and oxygen fugacity. The solid lines delineate the stability fields of Pb—O phases; dashed extensions are estimates beyond the range of direct experimental measurement. The Pb—O data are from White and Roy (1964) and Otto (1966). Also shown as dotted lines are the positions of familiar "geologic" buffer curves in the iron-oxygen system: MH = magnetite-hematite; WM = wüstite-magnetite; IW = iron-wüstite. For present purposes, the important point is that PbO (i.e., Pb^{2+}) is stable when oxygen fugacity is buffered at MH, as in our experiments and most banded iron formations.

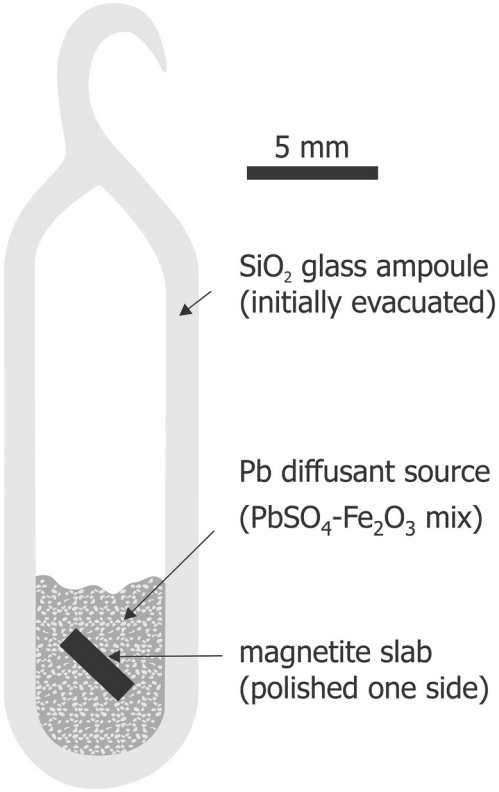

Fig. 2. Schematic representation of the container, sample, and source configuration for experiments on Pb diffusion in magnetite. See text for details.

source, which compromised the suitability of the surface for measuring diffusive uptake of Pb.

Most experiments were conducted on magnetite slabs cut parallel to {001}, but two samples oriented parallel to {111} were also run to confirm the isotropic character of Pb diffusion in magnetite, which is expected of a crystal belonging to the isometric (cubic) crystal system. A time series of experiments spanning 75–476 h was conducted at 650 °C to establish that the measured Pb diffusivity is independent of experiment duration.

Table 2
Summary of Pb diffusion experiments and results.

Expt. No.	T(C)	time (h)	D (m^2/s)	logD	σ
PbMt-2	600	405	1.03×10^{-22}	−21.99	0.13
PbMt-3	500	2035	2.09×10^{-23}	−22.68	0.27
PbMt-4	675	94	5.00×10^{-22}	−21.30	0.17
PbMt-5	550	815	9.33×10^{-23}	−22.03	0.16
PbMt-8a	620	331	1.60×10^{-22}	−21.80	0.20
PbMt-8b	620	331	1.24×10^{-22}	−21.91	0.22
PbMt-10	650	260	3.90×10^{-22}	−21.41	0.22
PbMt-11	580	1200	4.81×10^{-23}	−22.32	0.17
PbMt-12	530	1179	4.00×10^{-23}	−22.40	0.11
PbMt14a	650	74.5	2.88×10^{-22}	−21.54	0.37
PbMt-15a	650	476	1.27×10^{-22}	−21.90	0.16
PbMt-15b	650	476	3.84×10^{-22}	−21.42	0.13

3.2. Analytical

Following recovery of the magnetite slabs from air-quenched glass ampoules, they were sonicated in ethanol and evaluated for surface integrity (i.e., lack of obvious reaction with the Pb source) using optical microscopy. The samples were then depth-profiled perpendicular to the polished surface using Rutherford backscattering spectroscopy (RBS) at the Dynamitron accelerator in the Ion Beam Laboratory at the University at Albany (SUNY). RBS is well suited to the present study because the technique is most sensitive for characterization of high-mass impurities in a relatively light matrix. A $^4He^+$ beam of energy 2 MeV was used for RBS analyses, with a solid-state surface barrier detector used to detect backscattered He. Beam spots were typically about $1mm^2$. We achieved a detection limit for Pb of ~50 ppm and a spatial (depth) resolution of ~10 nm. A typical RBS spectrum is presented in Fig. 3, where the peak representing in-diffused Pb is seen to be well separated from the Fe edge. Note that the energy of a backscattered He ion (proportional to channel number in the spectrum) depends positively on the mass of the scattering nucleus and negatively on the depth in the sample at which the scattering event occurs. It is the latter effect that enables depth-profiling for concentration.

The Pb spectral feature is readily converted to a concentration profile (see Cherniak and Watson, 2001), two examples of which are shown in Fig. 4a & b. Lead diffusivities were extracted from the concentration

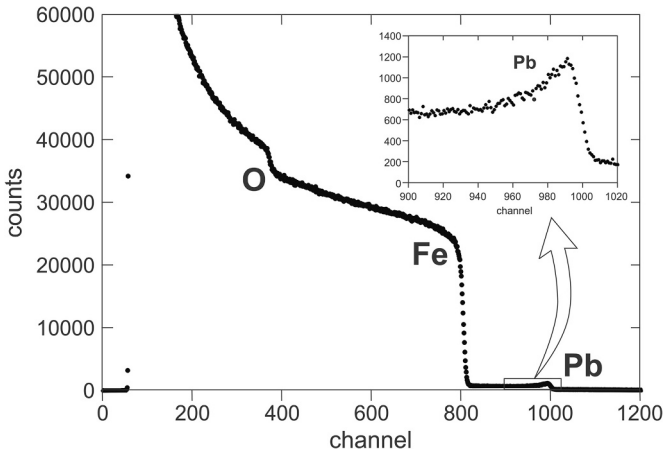

Fig. 3. A typical Rutherford backscattering (RBS) spectrum obtained by depth-profiling a magnetite crystal surface into which Pb was diffused from a surface source (see Fig. 2). The Pb feature is small because of the low concentration of Pb, but the enlargement at the upper right reveals the monotonic diminution of Pb progressing into the crystal from the surface at the right. See text for RBS details.

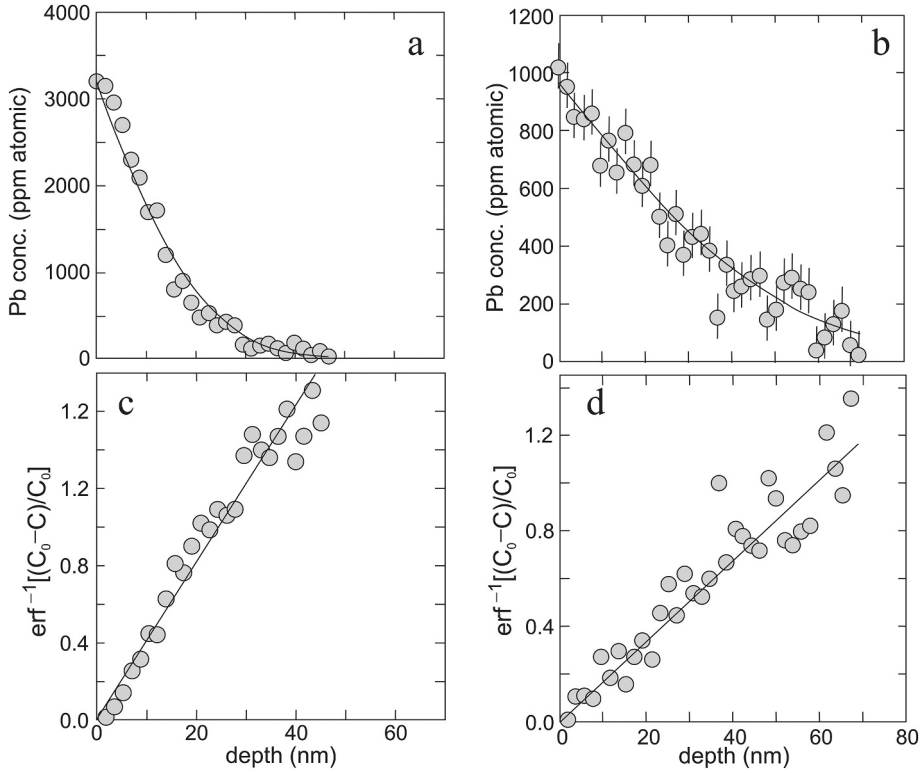

Fig. 4. (a & b) Two examples of Pb "in-diffusion" profiles obtained from experimentally treated magnetite crystals: (a) Shows one of the shortest profiles obtained in this study (run PbMt-2); (b) is one of the longest (run PbMt-12). The curves are error-function fits to the data, obtained by assuming conformance with eq. 1. (c & d) are linearized versions of a & b, respectively, in which the raw concentration data have been inverted through the error function. Diffusivities are calculated from the slopes of the linearized data plots, as discussed in the text.

profiles by invoking the solution to the non-steady state diffusion equation in 1 dimension for the specific case of diffusion into a semi-infinite medium from a planar surface at which Pb concentration remains constant over time. The relevant solution for these boundary conditions is

$$\frac{C(x,t)}{C_0} = 1 - erf\left(\frac{x}{\sqrt{4D_{Pb}t}}\right) \quad (1)$$

where $C(x,t)$ is the concentration of Pb at distance x from the surface and time t, C_0 is the concentration at the surface, and D_{Pb} is the diffusivity of Pb in the magnetite structure. Concentration versus depth data from RBS analysis of a magnetite slab were inverted through the error function (i.e., by plotting erf^{-1}(1-C/C_0) vs. x) to obtain an expected linear array (Fig. 4c & d). Linear regression yielded a slope ($= -1/\sqrt{4D_{Pb}t}$) and diffusivity from this plot.

4. Results and discussion

4.1. Data systematics

Lead diffusivities recovered from 12 experiments are listed in Table 2 and plotted in Fig. 5, which includes ±1σ uncertainties in D_{Pb} values based upon the slope uncertainties of the raw data plots described above. Least-squares fitting of logD_{Pb} versus reciprocal absolute temperature (T) yields an Arrhenius-type relation:

$$D_{Pb}\left(m^2 \bullet s^{-1}\right) = D_0 exp[-E_a/RT] \quad (2)$$

where R is the gas constant. The pre-exponential constant (D_0) has a value of 9×10^{-17} m^2·s^{-1} (±6%) and the activation energy (E_a) is 98,000 J·mol^{-1} (±15%).

Figure 6 shows four Pb diffusivities resulting from a time series of

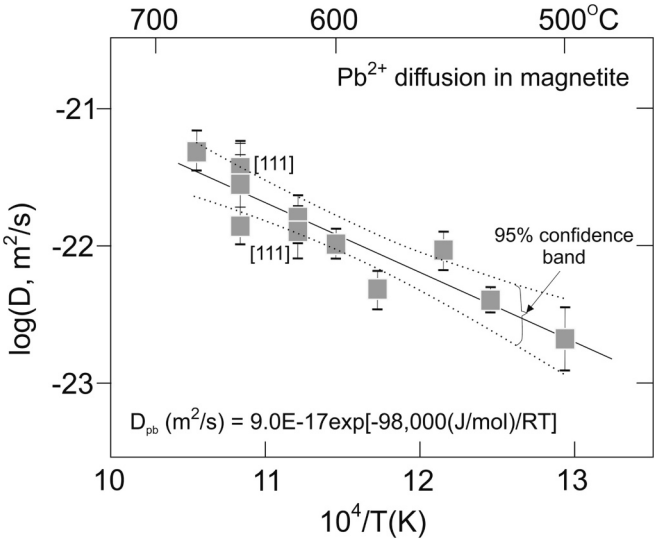

Fig. 5. Summary of Pb diffusivities on an Arrhenius-type plot. All measurements except the two labeled otherwise involved Pb diffusion perpendicular to {100}. Error bars represent ±1σ uncertainties in the slopes of plots like those shown in Fig. 4c & d. The 95% confidence band is indicated by the dotted curves. See text for discussion and Table 2 for a summary of experiments and results.

experiments conducted at 650 °C. Three values from experiments of 75, 260 and 476 h duration are indistinguishable within uncertainty. The value obtained from a separate 476-h experiment is slightly low relative to the other three, but is nevertheless in agreement at the ±2σ level. Importantly, there is no suggestion of systematic time dependence of the

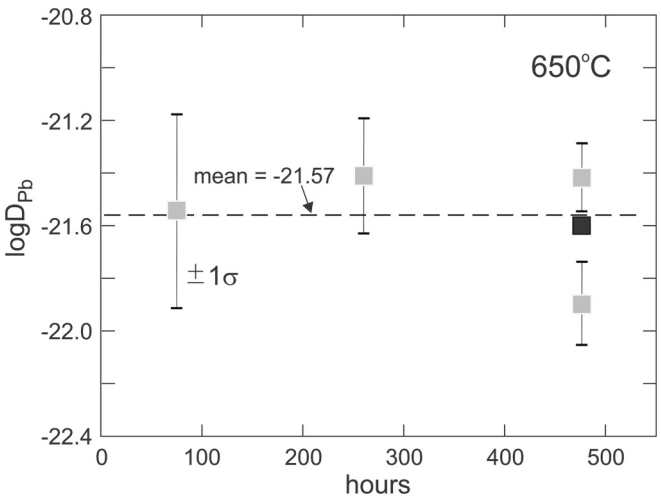

Fig. 6. Lead diffusivities resulting from a series of experiments of varying duration conducted at 650 °C. The lack of time dependence is indicative of diffusion control of Pb transport. The black square is the average of the two experiments of the same duration.

data, which is consistent with Pb transport in magnetite by volume diffusion.

In Fig. 7, results for Pb diffusion in magnetite are shown in comparison with diffusion laws from the literature for Al, Ti, Cr, Mn, Fe, Co and Ni in magnetite (Van Orman and Crispin, 2010), all characterized at an f_{O2} corresponding to MH. The previous studies were conducted at much higher temperatures than the present investigation, so detailed comparison of diffusion relationships is of limited value. However, down-*T* extrapolation of published Arrhenius laws to the ~500–700 °C range of our study suggests diffusivities for most cations that are orders of magnitude higher than that of Pb. Chromium is a possible exception; in this case—because E_a for Cr diffusion is relatively high—down-T extrapolation places Cr diffusivities in the vicinity of our Pb values at 500–600 °C. Note that the activation energy for Pb diffusion (98 kJ/mol) is quite low relative to E_a for other cations. This raises the possibility that an extrinsic (defect-related) diffusion mechanism is in play for Pb, which would make up-temperature extrapolation of our Arrhenius law beyond the range of measurements somewhat risky. Fortunately, the temperature range of many geologic applications (including those involving BIFs) falls within or below the temperature span of our experiments (see section 4.2).

A useful conclusion from Fig. 7 is that Fe diffusion in magnetite at the temperatures of our experiments (estimated by down-T extrapolation) is 5–6 orders of magnitude faster than Pb diffusion. If, as we suspect, Pb^{2+} diffuses in magnetite by exchange with Fe^{2+}, it seems clear that Pb—Fe interdiffusion is not rate-limited by Fe mobility.

Figure 8 is a compilation of experimentally determined Arrhenius laws for Pb diffusion in a variety of minerals of geochronological interest, including highly refractory accessory phases such as monazite and zircon, as well as major rock-forming silicates and carbonates. Interestingly, the diffusion law for Pb in magnetite is most similar to that of Pb in calcite, although *D* values coincide with other minerals at specific temperatures due to crossing of Arrhenius lines (e.g., magnetite with apatite at ~600 °C, and magnetite with K feldspar and titanite at ~700 °C).

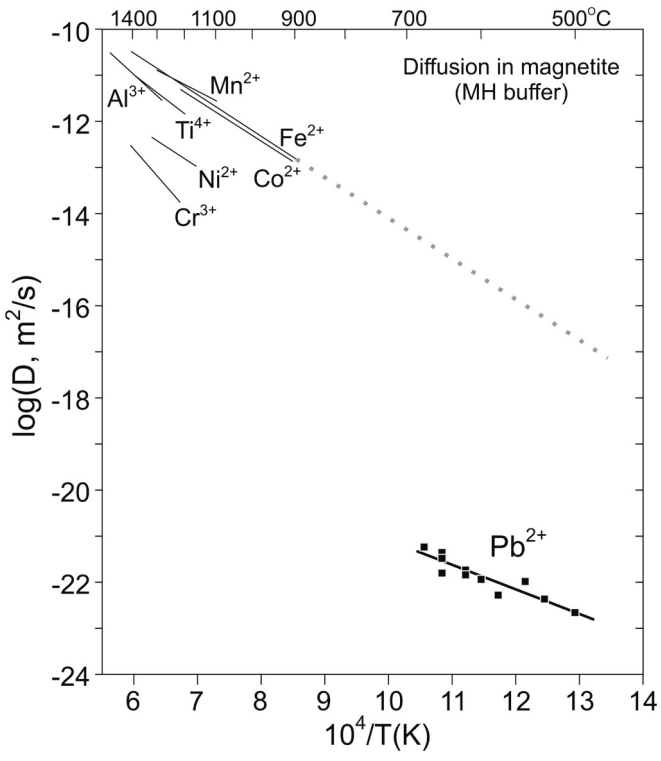

Fig. 7. Diffusion data from the literature (upper left) compared with present measurements for Pb (lower right). All data were obtained at oxygen fugacities corresponding to the MH buffer. With the possible exception of Cr, down-temperature extrapolation of most Arrhenius laws to 500–700 °C indicates diffusivities much higher that than of Pb. The Fe^{2+} line is extended to low temperature (gray dotted line) to emphasize that Pb—Fe interdiffusion is probably not rate-limited by Fe in our experiments. See Van Orman and Crispin (2010) for data sources.

4.2. *Pb retention in magnetite: diffusive closure and opening*

Equipped with an Arrhenius relation for Pb diffusion in magnetite, we can now evaluate the retention of radiogenic Pb in natural magnetite crystals subjected to geologic cooling, heating or thermal cycling. The

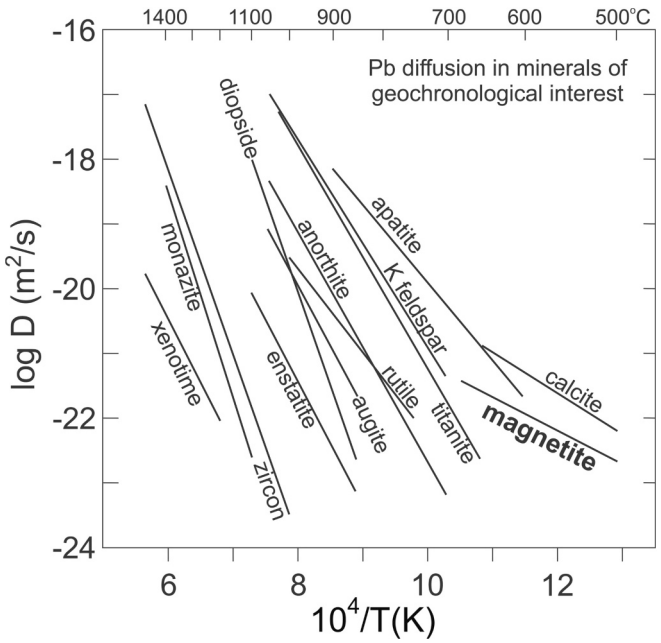

Fig. 8. Summary of Pb diffusion laws for a variety of minerals compared with that of magnetite. Data sources: anorthite (Cherniak, 1995), apatite (Cherniak et al., 1991), augite (Cherniak 2002), calcite (Cherniak, 1997), diopside (Cherniak, 1998), enstatite (Cherniak, 2001), K feldspar (Cherniak, 1995), monazite (Cherniak et al., 2004), rutile (Cherniak, 2000), titanite (Cherniak, 1993), xenotime (Cherniak, 2006), zircon (Cherniak et al. 2001).

usual first step in such an assessment is to calculate (by iteration) the closure temperature (T_C) according to the formula of Dodson (1973):

$$T_c = \frac{E_a/R}{ln\left[\frac{55RT_c^2(D_0/a^2)}{E_a(dT/dt)}\right]} \quad (3)$$

where E_a, R and D_0 are as defined for eq. 2, a is the radius of the diffusion domain, dT/dt is the cooling rate, and the constant 55 is a geometrical factor specific to a spherical diffusion domain. In principle, the diffusion domain for natural magnetites could be the entire crystal, but it is also possible that the domain is smaller due to the presence of fast diffusion pathways in the crystal. We note that the diffusion domain as defined here has no relationship to the magnetic domain state of the magnetite. The latter property reflects whether a grain is homogenously magnetized (single domain, which occurs for grains <~60 nm in diameter) or non-uniformly magnetized (pseudo single domain and multi-domain, which occurs for larger grains; [Nagy et al., 2017]).

The closure temperature given by eq. (3) applies strictly to cooling regimes in which temperature decreases at geologic rates in inverse proportion to time (e.g., as a banded iron formation cools after attaining peak metamorphic conditions). Fig. 9 shows T_C as a function of diffusion domain size and cooling rate. For large diffusion domain radii of 1 mm or greater, T_C can be as high as ~800 °C for rapidly-cooled systems (e.g., at 100 °C/MYr), but drops dramatically at slow cooling rates (e.g., 1 °C/MYr) and for smaller diffusion domain sizes that might better reflect those of some BIF magnetites. For diffusion domain radii on the order of 1 μm, for example, closure does not set in during cooling until the system reaches 150–200 °C. Nichols et al. (2023) estimated the diameters of magnetite grains in Isua BIF samples to fall in the range 1–27 μm. At the upper end of this size range, T_C is ~380 °C for cooling at 100 °C/MYr. This is well below the 580 °C Curie temperature for magnetite, which means that a Pb—Pb or U—Pb age determination could be more recent than the acquisition time of NRM. However, it still serves as a useful age for any subsequent thermal overprints that may have influenced the NRM after initial acquisition (see section 4.3).

Diffusive closure during cooling as described by the Dodson equation may be of limited usefulness for many BIFs because these rocks represent metamorphosed sediments that have experienced a thermal cycle. Magnetite grains in BIFs are generally believed to have crystallized

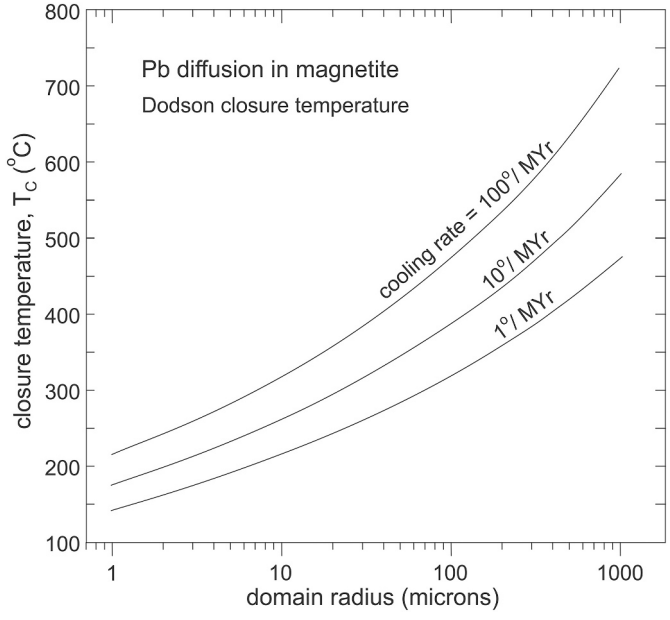

Fig. 9. Closure temperature (T_C) for Pb diffusion in magnetite as a function of cooling rate and diffusion domain radius, according to the Dodson formulation (eq. 3 in text). See text for discussion.

under diagenetic or low-grade metamorphic conditions (Rasmussen and Muhling, 2018; Konhauser et al., 2017; Nutman, 2017) where Pb is effectively immobile. However, partial or total open-system behavior of Pb could set in at any point during prograde metamorphism, which would greatly complicate the interpretation of U—Pb data. A protocol for assessing Pb mobility throughout a metamorphic cycle is essential, perhaps especially at temperatures near the magnetite Curie point.

The risk of relying on T_C to rule out diffusive loss during heating is starkly illustrated by the fact that 40% diffusive loss is the inevitable result of linear heating from ambient temperature up to Dodson's T_C (Cherniak and Watson, 2007; Watson and Cherniak, 2013). Such loss would result in an underestimate of age, and might not be recognizable on a Concordia diagram because of its gradual nature. Fortunately, diffusive loss can be quantified for any heating scenario if the Arrhenius law (E_a and D_0) for the diffusant of interest is known. Cherniak and Watson (2007) and Gardés and Montel (2009) provided equations that describe diffusive opening in a manner broadly analogous to that of Dodson (1973) for closure during cooling. Watson and Cherniak (2013) presented, in addition, a general equation that gives the specific extent of diffusive loss during linear heating to any temperature of interest. For linear heating ($T \propto$ time), diffusive opening is described by

$$T_{rt}\% = \frac{0.457 \bullet (E_a/R)}{\chi_h + log\left[\frac{E_a \bullet D_0}{R \bullet dT/dt \bullet a^2}\right]} - 0.8 \quad (4)$$

where $T_{rt\%}$ is the temperature (in kelvins) at which a specific fractional retention occurs, which coincides with a specific value of the constant χ_h. For example, χ_h has a value of 2.756 for 99% retention during heating; χ_h values for retention levels ranging from 0.1 to 99.9% are provided in Watson and Cherniak (2013). Fig. 10 shows temperatures corresponding to 50, 80, 99 and 99.9% retention of Pb as a function of diffusion domain size at linear heating rates of 10° and 100°/MYr. Note that 99% Pb retention (1% diffusive loss) occurs at ~350°-375 °C for 1-μm diffusion domains and ~ 575°-650 °C for 1-mm diffusion domains (see Fig. 10b). A substantial fraction of Pb is retained to considerably higher temperatures (see 80% and 50% curves in Fig.10c and d), but the U—Pb isotopic system is clearly compromised in these cases.

In the context of BIF thermal evolution, the most relevant diffusive opening scenarios might be closed-loop events (i.e., complete thermal cycles that include both prograde and retrograde metamorphism). Watson and Cherniak (2013) developed general equations that can be used to calculate the extent of diffusive loss during such events, including linear heating followed immediately by linear cooling (a "steeple" time-temperature path), as well as parabolic t-T paths. Here we briefly consider the parabolic case. Fractional loss over a parabolic time-temperature path can be obtained from the following relationship:

$$\log\zeta = log\left[\frac{D_o\tau}{a^2}\right] + \frac{140}{T_{pk}} - \frac{0.437E_a}{RT_{pk}} - 0.8 \quad (5)$$

where $\zeta = a^{-2}\int_{t=0}^{\tau} D(t)dt$, τ is the duration of the heating event (in seconds) and T_{pk} is the peak temperature in kelvins (see Fig. 11 inset). The total fractional loss (F) is uniquely determined by the value of ζ; conversion of log ζ to F is straightforward using tabulated or graphical information found in Watson and Cherniak (2013). Fig. 11 shows fractional Pb loss as a function of T_{pk} and diffusion domain size during a parabolic thermal event lasting 30 MYr. For a diffusion domain radius of 1 mm, total Pb loss is negligible for $T_{pk} \approx$ 200 °C and ~ 8% for $T_{pk} \approx$ 400 °C. Smaller diffusion domain sizes lead to more significant Pb loss over the same parabolic thermal event. For example, 10 μm diffusion domains result in ~8% Pb loss for a modest peak temperature of 170 °C.

A few general observations may be helpful in closing this section. First, it should be noted that in-growth of Pb is not taken into account by any of the equations used to assess diffusive closure and opening. In-growth of Pb would be minimal over the time scales considered above, so this particular shortcoming will be relatively minor for most

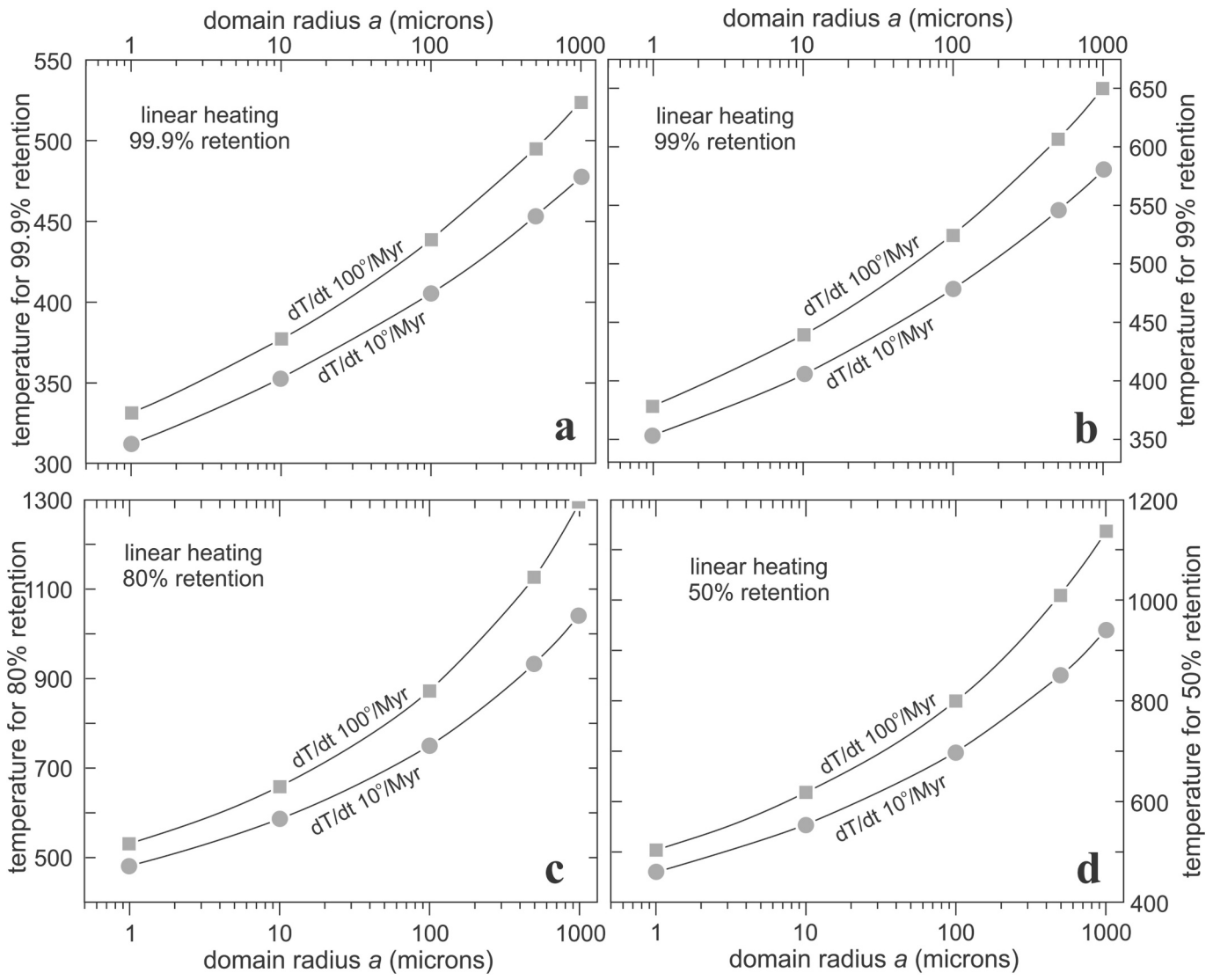

Fig. 10. Diagrams illustrating diffusive opening of Pb in magnetite as a consequence of heating ($T \propto t$) at rates of 10 and 100 °C/MYr. The plotted temperatures correspond to 99.9, 99, 80 and 50% Pb retention, respectively, in panels a, b, c, and d. Note the strong dependence of opening behavior upon the radius of the diffusion domain. These plots were generated using eq. 4; see text for details and discussion.

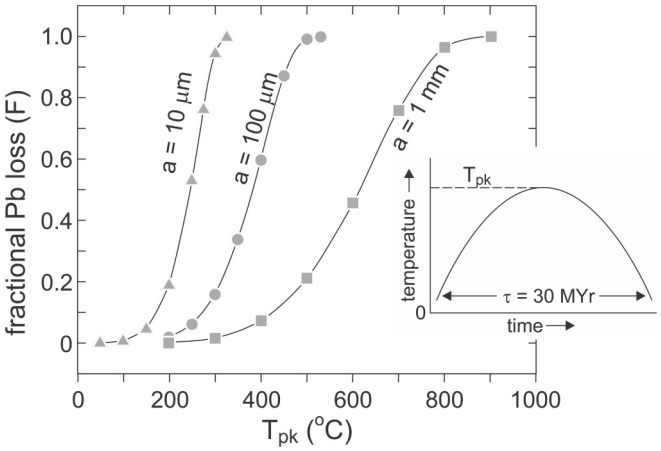

Fig. 11. Fractional loss of Pb from magnetite as a function of the peak temperature (T_{pk}) achieved during a 30-MYr parabolic heating event, computed using eq. 5. See *T-t* inset and text for discussion.

BIF *t-T* scenarios. A far greater concern is the lack of constraints on the radius (a) of diffusion domains in natural magnetite crystals. Because the overall diffusive response depends upon a^2, this parameter has a large effect on closure and opening systematics (see Figs. 9-11). This limitation is particularly vexing due to the added complication of possible time dependence of the diffusion domain radius during a thermal event of interest. For example, general coarsening of magnetite grains during prograde metamorphism might tend to increase the diffusion domain size over time, improving Pb retention. Stress-induced deformation, on the other hand, could have the opposite effect by introducing extended defects into the magnetite crystal structure that could serve as fast paths for diffusion, decreasing the effective size of Pb diffusion domains and jeopardizing Pb retention. See Supplementary document S3 for a detailed discussion of grain sizes of natural magnetites.

A final noteworthy consideration is that our new diffusion law for Pb in magnetite, like all experimentally characterized phenomena, comes with significant uncertainty—especially in the activation energy E_a (see eq. 2 and Fig. 5). This uncertainty means that diffusion of Pb may be somewhat more or less effective at an assumed geologic model temperature than is indicated by the value of D_{Pb} given by eq. 2. The

consequences of the uncertainty in D_{Pb} for diffusive Pb loss from a magnetite sphere are illustrated in Fig. 12. Due to the "bow tie" shape of the 95% confidence band in Fig. 5 (widest at ~500 °C), the range of possible diffusive loss due to uncertainty in D_{Pb} is largest at this temperature, amounting to ~20%. Considering the uncertainty in system characteristics such as grain size and temperature, this range seems fairly modest.

4.3. Dating BIFs and the timing of NRM acquisition

The challenges above aside, it is instructive to consider the interplay of Pb diffusion behavior and the acquisition and subsequent thermal overprinting of NRM over some hypothetical BIF time-temperature histories. This topic is especially interesting given the great age of some BIFs and the possibility that such rocks might document the early existence of an intrinsic terrestrial magnetic field (Nichols et al., 2023.). Fig. 13 illustrates four broadly parabolic time-temperature paths beginning with BIF precipitation in the deep geologic past. In due time the newly-formed BIF is heated (through burial) to a hypothetical peak temperature and then cooled back to Earth's surface temperature (through uplift and erosion) over an unspecified time interval. Because the Pb diffusion domain size is unknown, the opening temperatures are also hypothetical and are deliberately varied among the four scenarios considered. In cases 1–3, magnetite is assumed to be present from its diagenetic origin onward, with implicit coarsening throughout the cycle. In case 4, magnetite crystallization is delayed until mid-metamorphic grade on the prograde limb, at which time coarse crystals are formed.

Case 1 in Fig. 13 is the simplest of the four scenarios because the peak temperature exceeds neither the opening temperature for Pb diffusion in magnetite nor its Curie temperature. In this case, a U—Pb or Pb—Pb age determination would reflect the formation age of the BIF, and the highest blocking temperature fraction of the NRM carried by single domain magnetite could provide a record of the existence of a terrestrial magnetic field at that time.

Case 2 in Fig. 13 is more complicated because the diffusive opening temperature for Pb is exceeded as the BIF progresses along its hypothetical *t-T* path. The severity of Pb loss could be assessed based on assumed values of the parameters in eq. 5, but any amount of Pb loss would only allow a lower limit on the BIF deposition age. Ultimately, the diffusively-compromised BIF cools through the Dodson closure temperature (T_C), and it is this event that a radioisotopic age would reflect. An additional feature of Case 2 is that the Curie temperature of magnetite is not exceeded, so detected NRM could have been acquired during diagenetic magnetite growth shortly after BIF precipitation. This case illustrates the interesting possibility that NRM acquisition could predate the apparent radiometric age of a BIF, and the radiometric age would correspond to a low temperature overprint that can be effectively removed during thermal demagnetization for single-domain magnetite grains.

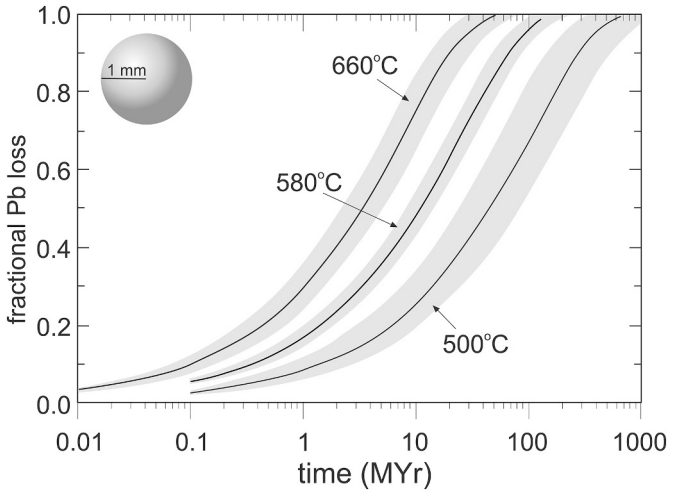

Fig. 12. Illustration of the effect of uncertainty in Pb diffusion parameters (D_0 and E_a) upon estimated Pb loss from a magnetite sphere of 1 mm radius held at 500°, 580° or 660 °C. The heavy black lines were computed using diffusivities given by eq. 2. The gray envelopes reflect the uncertainty in *D* as indicated by the 95% confidence band in Fig. 5. Note that smaller or larger magnetite crystals (spheres) would yield the same relative differences but with a compressed or expanded time axis.

The third hypothetical *t-T* path (Case 3 in Fig. 13) considers a BIF containing diffusively retentive magnetite—attributable, perhaps, to the presence of large diffusion domains and/or rapid heating. For the *t-T* path shown, the Curie temperature of magnetite is exceeded but the opening temperature for Pb diffusion is not. The radiometric age of magnetite from this sample would reflect the actual deposition age of the BIF, but NRM present in a recovered sample would have been acquired later as the rock cooled back through the Curie temperature.

Our final *t-T* scenario (Case 4 in Fig. 13) differs from the previous three in that crystallization of magnetite—rather than being diagenetic—is delayed until intermediate-grade metamorphic conditions are achieved. This case is both plausible and interesting because the resulting magnetite crystals can be assumed to be relatively large and therefore more retentive of Pb than low-T precipitates. Given the existence of a terrestrial magnetic field, NRM would be imprinted at the time of magnetite growth. If radiogenic Pb is fully retained and the Curie temperature is not exceeded, the measured age would accurately reflect the initial BIF metamorphism *and* the existence of a terrestrial magnetic field.

Based on our new Pb diffusion law, all four time-temperature scenarios illustrated in Fig. 13 represent plausible relationships between the Curie temperature and diffusion of radiogenic Pb in BIF magnetite. These examples are not exhaustive, and readers will certainly identify additional possibilities. The crucial realization is that many realistic geologic *t-T* paths can preserve true BIF ages as well as the initial NRM acquisition, but well-constrained estimates of the duration and peak temperature of BIF metamorphism are key to evaluating any natural situation. Also, as noted previously, the size of Pb diffusion domains in magnetite is a crucial factor in Pb retention. The study of Isua BIF by Nichols et al. (2023) suggests consistency between the actual grain size of magnetite crystals and the size of Pb diffusion domains, which is another promising indicator of the usefulness of BIF magnetite in studies of the early history of our planet.

The main conclusion of this study is that Pb^{2+} diffusion in magnetite is substantially slower than might be inferred from previous data for other cations. This finding is encouraging in terms of the potential for BIF magnetites to yield reliable U—Pb age information, which in some cases will be relatable to paleomagnetic measurements. It must be acknowledged that some geologic scenarios are conducive to open-system behavior of Pb in magnetite and resetting of radioisotopic ages; however, our diffusion law provides a basis for distinguishing between promising and less promising situations. The exciting aspect of our results is that the classical Dodson closure temperature (T_C) for realistic diffusion domain sizes and cooling rates is fortuitously close to the 580 °C Curie point of magnetite, which makes the U—Pb system a unique and potentially powerful tool for dating BIF magnetites and the initiation of Earth's dynamo.

Declaration of Competing Interest

The authors declare the following financial interests/personal relationships which may be considered as potential competing interests:

Benjamin Weiss reports financial support was provided by Heising-Simons Foundation.

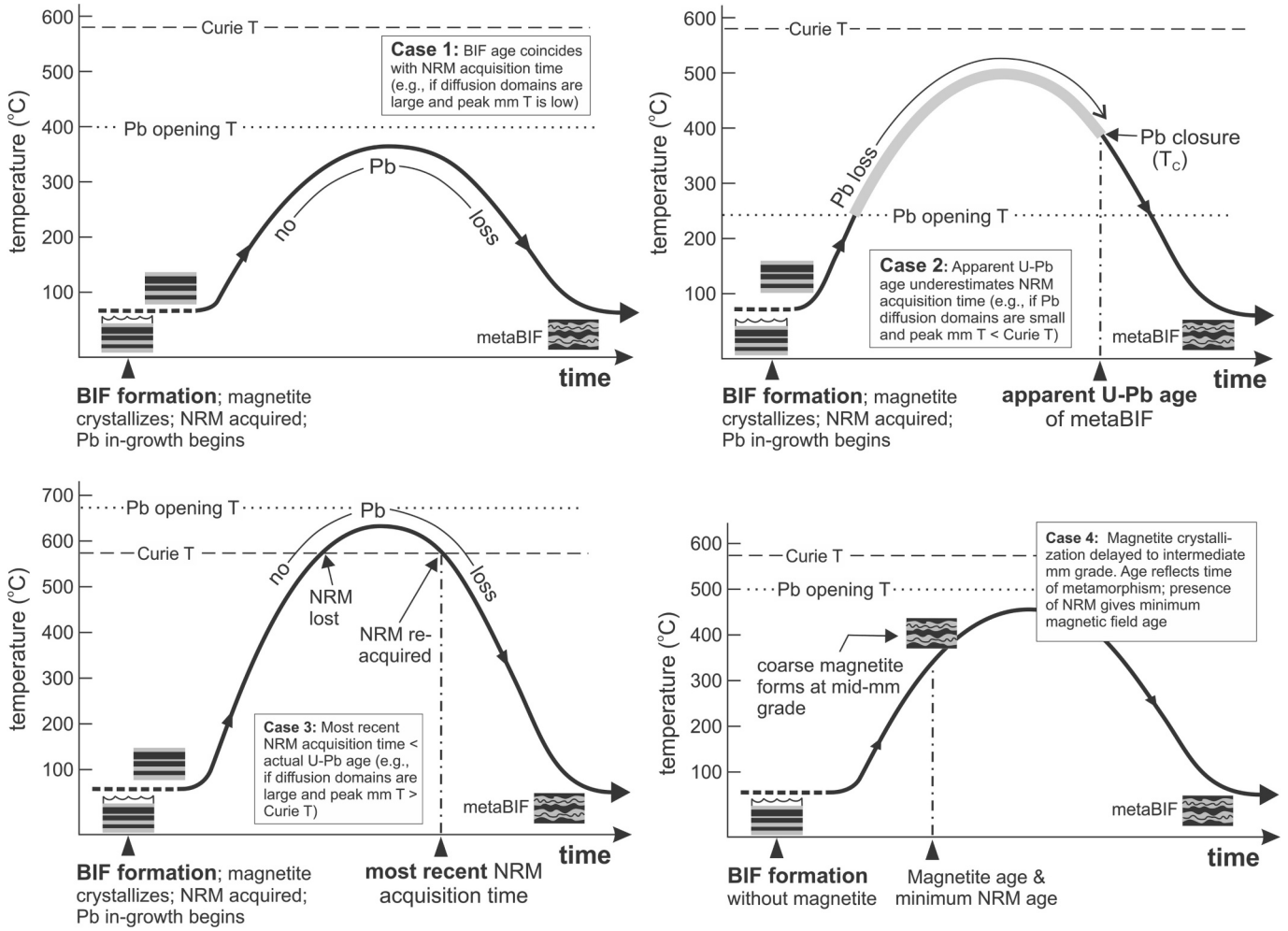

Fig. 13. Four time-temperature scenarios illustrating the possible interplay between the Curie temperature of magnetite and opening/closure with respect to Pb diffusion. In cases 1–3 magnetite is assumed to form during BIF precipitation; in case 4, magnetite crystallization is delayed to intermediate metamorphic grade where large crystals are formed. The Pb opening temperature differs among these cases because it depends upon diffusion domain size. See text for discussion.

Data availability

Data will be made available on request.

Acknowledgements

BPW and CION are grateful for the support of the Heising-Simons Foundation through grant no. 556352. EBW and DJC acknowledge Rensselaer Polytechnic Institute for contributing analytical costs at the Ion Beam Laboratory at the University at Albany. Oliver Wolfe and Jen Gorce kindly provided the EPMA analyses of the Moriah magnetite.

Appendix A. Supplementary data

Supplementary data to this article can be found online at https://doi.org/10.1016/j.chemgeo.2023.121748.

References

Cherniak, D.J., 1993. Lead diffusion in titanite and preliminary results on the effects of radiation damage on Pb transport. Chem. Geol. 110, 177–194.
Cherniak, D.J., 1995. Diffusion of Pb in plagioclase and K-feldspar measured by Rutherford Backscattering spectroscopy and resonant nuclear reaction analysis. Contrib. Mineral. Petrol. 120, 358–371.
Cherniak, D.J., 1997. An experimental study of Sr and Pb diffusion in calcite, and implications for carbonate diagenesis and metamorphism. Geochim. Cosmochim. Acta 61, 4173–4179.
Cherniak, D.J., 1998. Pb diffusion in clinopyroxene. Chem. Geol. 150, 105–117.
Cherniak, D.J., 2000. Pb diffusion in rutile. Contrib. Mineral. Petrol. 139, 198–207.
Cherniak, D.J., 2001. Pb diffusion in Cr diopside, augite, and enstatite, and consideration of the dependence of cation diffusion in pyroxene on oxygen fugacity. Chem. Geol. 177, 381–397.
Cherniak, D.J., 2006. Pb and rare earth element diffusion in xenotime. Lithos 88, 1–14.
Cherniak, D.J., Watson, E.B., 2001. Pb diffusion in zircon. Chem. Geol. 172, 5–24.
Cherniak, D.J., Watson, E.B., 2007. Ti diffusion in zircon. Chem. Geol. 242, 473–486.
Cherniak, D.J., Lanford, W.A., Ryerson, F.J., 1991. Lead diffusion in apatite and zircon using ion implantation and Rutherford Backscattering techniques. Geochim. Cosmochim. Acta 55, 1663–1673.
Cherniak, D.J., Watson, E.B., Grove, M., Harrison, T.M., 2004. Pb diffusion in monazite: a combined RBS/SIMS study. Geochim. Cosmochim. Acta 68, 829–840.
Courtney-Davies, L., Danisik, M., Ramanaidou, E.R., Kirkland, C.L., Evans, N.J., Piechocka, A.M., McInnes, B.I.A., 2022. Hematite geochronology reveals a tectonic trigger for iron ore mineralization during Nuna breakup. Geology 50, 1318–1323.
Dodson, M.H., 1973. Closure temperature in cooling geochronological and petrological systems. Contrib. Mineral. Petrol. 40, 259–274.
Erel, Y., Harlavan, Y., Stein, M., Blum, J.D., 1997. U-Pb dating of Fe-rich phases using a sequential leaching method. Geochim. Cosmochim. Acta 61, 1697–1703.
Frei, R., Polat, A., 2007. Source heterogeneity for the major components of 3.7 Ga Banded Iron Formations (Isua Greenstone Belt, Western Greenland): tracing the nature of interacting water masses in BIF formation. Earth Planet. Sci. Lett. 253, 266–281.
Frei, R., Bridgwater, D., Rosing, M., Stecher, O., 1999. Controversial Pb-Pb and Sm-Nd isotope results in the early Archean Isue (West Greenland) oxide iron formation: Preservation of primary signatures versus secondary disturbances. Geochim. Cosmochim. Acta 63, 473–488.
Gardés, E., Montel, J.M., 2009. Opening and resetting temperatures in heating geochronological systems. Contrib. Mineral. Petrol. 158, 185–195.
Klein, C., 2001. Presidential address to the Mineralogical Society of America, Boston, November 6, 2001: some Precambrian Banded Iron-Formations (BIFs) from around

the world: their age, geologic setting, mineralogy, metamorphism, geochemistry, and origin. Am. Mineral. 90, 1473–1499.
Konhauser, K.O., Planavsky, N.J., Hardisty, D.S., Robbins, L.J., Warchola, T.J., Haugaard, R., Lalonde, S.V., Partin, C.A., Oonk, P.B.H., Tsikos, H., Lyons, T.W., Bekker, A., Johnson, C.M., 2017. Iron formations: a global record of Neoarchaean to Palaeoproterozoic environmental history. Earth Sci. Rev. 172, 140–177.
Nagy, L., Williams, W., Muxworthy, A.R., Shcherbakov, V.P., 2017. Stability of equidimensional pseudo–single-domain magnetite over billion-year timescales. Proc. Natl. Acad. Sci. 114 (39), 10356–10360.
Nichols, C.I.O., Weiss, B.P., Eyster, A., Martin,C.R., Maloof, A.C., Kelly, N.M., Zawaski, M.J., Mojzsis, S.J., Watson, E.B., Cherniak, D.J., 2023. An Eoarchean record of the geomagnetic field preserved in the Isua Supracrustal Belt, Southwest Greenland. Submitt. J. Geophys. Res.; Doi:10.31223/X5SX0V.
Nutman A.P., 2017. Isua stromatolites - Understanding the Field Setting. Technical Report, University of Wollongong. Doi:10.13140/RG.2.2.13602.63681.
Otto, E.M., 1966. Equilibrium pressures of oxygen over oxides of lead at various temperatures. J. Electrochem. Soc. 113, 525–527.
Rasmussen, B., Muhling, J.R., 2018. Making magnetite late again: evidence for widespread magnetite growth by thermal decomposition of siderite in Hamersley banded iron formations. Precambrian Res. 306, 64–93.
Van Orman, J.A., Crispin, K.L., 2010. Diffuson in oxides. Rev. Mineral. Geochem. 72, 757–825.
Watson, E.B., Cherniak, D.J., 2013. Simple equations for diffusion in response to heating. Chem. Geol. 335, 93–104.
Watson, E.B., Cherniak, D.J., Thomas, J.B., Hanchar, J.M., Wirth, R., 2016. Crystal surface integrity and diffusion measurements on Earth and planetary materials. Earth Planet. Sci. Lett. 450, 346–354. https://doi.org/10.1016/j.epsl.2016.06.043.
White, W.B., Roy, R., 1964. Phase relations in the system lead-oxygen. J. Am. Ceram. Soc. 47, 242–249.